# V. RESULTS AND DISCUSSION

## A. PRESSURE GRADIENT

Maintenance of a zero pressure gradient on plates for boundary layer testing has long been a major problem. Due to variations in the dimensions of the wind tunnel test section, growth of the boundary layer on the wind tunnel walls and the test article itself, and the effect of holes and imperfections in the tunnel walls, the static pressure along the plate usually needs some correction to bring it close to a zero pressure gradient condition. Klebanoff and Diehl[29], in one of their earlier investigations took measurements of static pressure along a test plate and attempted to obtain a zero pressure gradient through the use of an adjustable false wall in the test section above the test plate. Figure 17 illustrates their final pressure distribution along the plate, which they viewed as adequate. Since their early results follow closely the boundary layer models available today, it can be concluded that they were correct in that assumption.

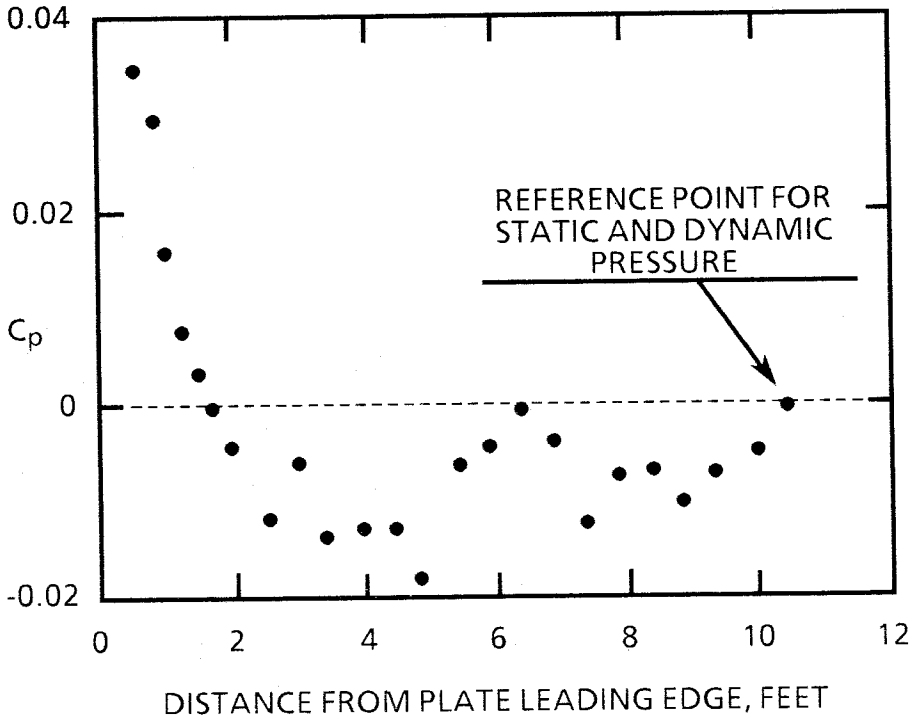


Figure 17 - Pressure distribution of Klebanoff and Diehl's experiment.

Table I - Profile Coordinates of False Wall 'D'

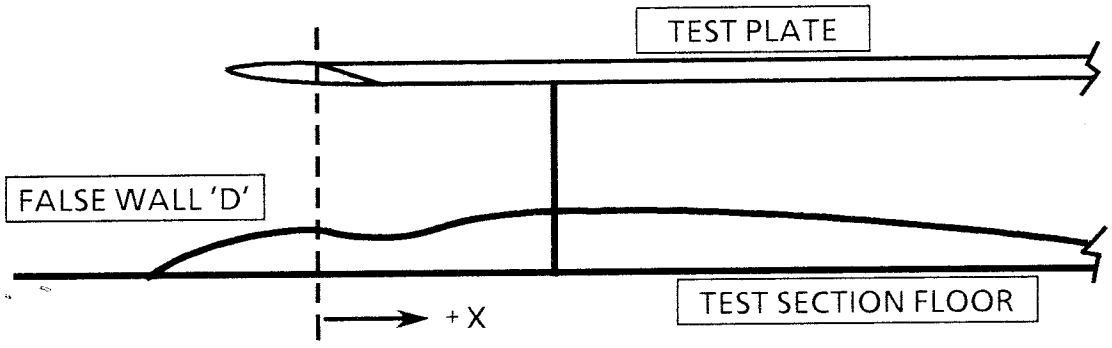


| X, INCHES | FALSE WALL THICKNESS, INCHES |
|---|---|
| 0.00 | 1.46 |
| 2.25 | 1.35 |
| 5.00 | 1.38 |
| 7.75 | 1.65 |
| 12.50 | 1.69 |
| 18.50 | 1.55 |
| 26.00 | 1.38 |
| 31.50 | 1.15 |
| 39.00 | 0.99 |
| 45.25 | 0.755 |
| 52.25 | 0.635 |
| 57.25 | 0.43 |
| 61.00 | 0.27 |
| 64.50 | 0.185 |
| 69.25 | 0.00 |

In this investigation many plate configurations were studied before an acceptable pressure distribution was obtained over the test plate. It was assumed that Klebanoff and Diehl had determined a good criterion for modeling a zero pressure gradient, which was no more than a 0.02 variation in pressure coefficient. It must be noted that their

reference condition taken ten and one-half feet from the leading edge of their test plate is not universal, or useful for comparison with experiments like this one. Since some acceleration of the flow did occur in Klebanoff and Diehl's experiment, their reference point produced a low apparent pressure coefficient difference along the plate. A more realistic reference point is at the leading edge of the plate, before the pressure variations occur. This more restrictive reference point was used in this investigation.

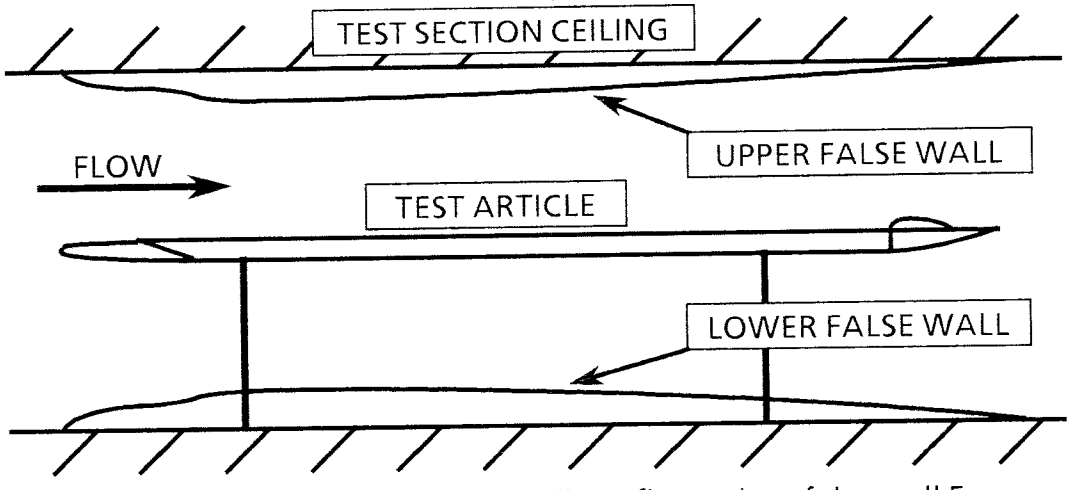


Figure 18 - Final twin false wall configuration, false wall F.

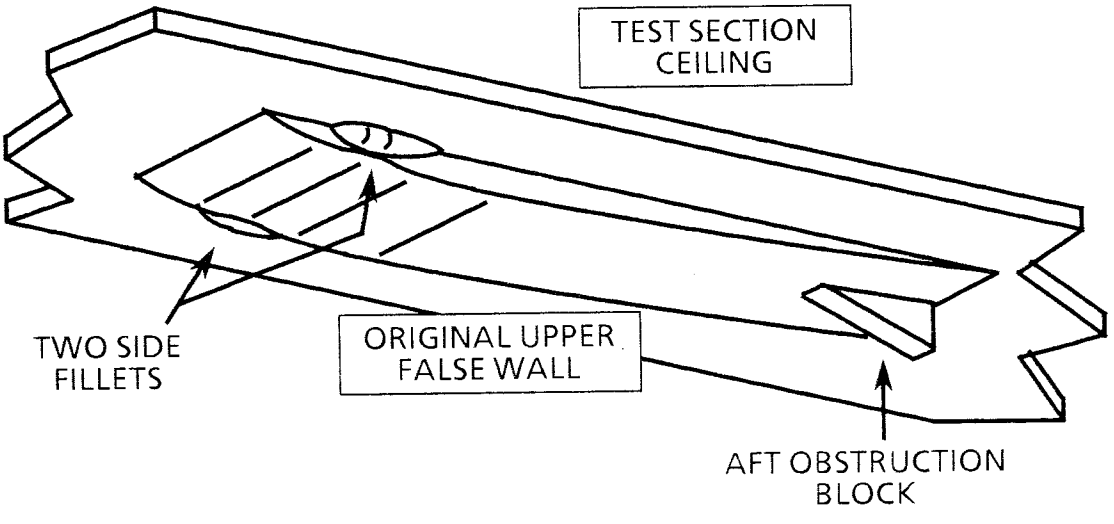


Figure 19 - Ceiling false wall with pressure gradient trim blocks, wall F

Detailed development of the test plate system with regard to obtaining a suitable pressure distribution is in Appendix A. A dual false wall system was used in the final plate configuration to control the pressure gradient. Each false wall was one foot in width. One wall was placed on the wind tunnel test section floor between the test plate support rods. The other was placed on the ceiling centerline, at the same axial station. The false wall profile thickness contour of the false walls are given in Table I. The general arrangement of the false walls is shown in Figure 18.

While the basic false wall treatment served to control most of the pressure variation, two small side fillets and an obstruction block were added to the upper false wall to obtain the final pressure distribution. These blocks are shown in Figure 19. The final pressure distribution shown in Figure 20 is completely satisfactory compared to the experiment of Klebanoff and Diehl.

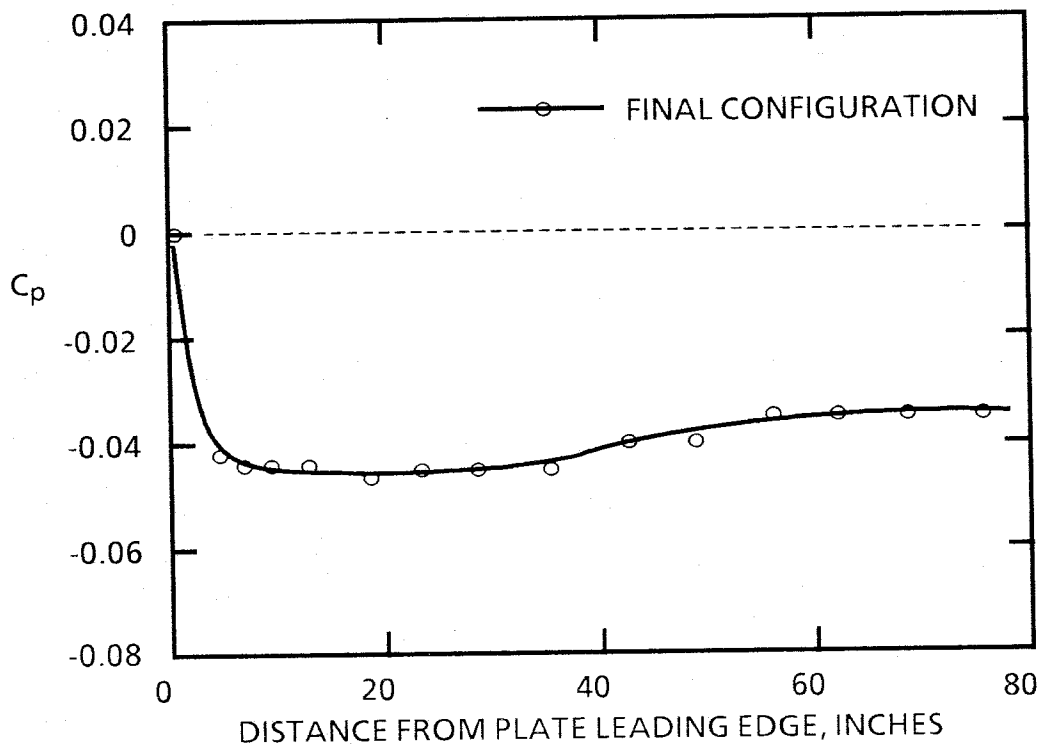


Figure 20 - Final pressure distribution.

## B. HOT-WIRE ANEMOMETER CALIBRATION

In order to take measurements of velocity and turbulence level in a fluid, some knowledge of the accuracy of the instrument used is necessary. In boundary layer measurements, in particular, the range of velocities is large, and some assurance is needed that the instrument will calibrate well from the full free stream value down to nearly zero velocity, while experiencing extreme dynamic fluctuations from the average velocity. Not enough work has been done in this area to provide clear specifications of hot-wire accuracy. Although many have performed comparitive tests of cylinder heat-transfer functions under static conditions, as Bradbury and Castro[65] did, few have tried to make statements about the accuracy and range of valid hot-wire anemometer measurements under dynamic conditions in the manner of Bruun[68]. Furthermore, published statistical studies of calibration are extremely rare, which is cause for some alarm. Few calibrations are not subject to random processes. It is necessary here to perform some simple analysis to determine the best caliberation method. Fortunately, in the course of the experiments, a large amount of calibration data has been taken, adequate to perform a fairly good statistical analysis.

There are basically three families of calibration functions that are evident in the literature. The three types are the power law, polynomial in square root of velocity, and King Series functions. The most widely used type is the power law, which is expressed as

$$E^2 = A + B \cdot V^n \qquad (32)$$

The exponent 'n' assumes different values in several works in the literature, although the most popular value is 1/2. Constants 'A' and 'B' are experimentally determined calibration constants for the particular hot-wire used. The results of Collis and Williams[64] show that the best value of 'n' is 0.45, while King originally derived the hot-wire calibration function with an exponent of 0.50. King's calibration function, known as King's Law, is also related

to the other two families of calibration functions, in fact a direct result of King's series solution for convection from a heated cylinder. This series can be expressed as

$$E^2 = A + B \times V^{0.5} + C \times V^{1.5} + D \times V^{2.5} + \ldots \qquad (33)$$

or

$$E^2 = A + B \times (V^{0.5}) + C \times (V^{0.5})^3 + D \times (V^{0.5})^5 + \ldots \qquad (34)$$

Apparently this function has not actually been applied in calibration of hot-wire anemometers, except in the first order King's Law form. The third family encompasses the empirical function found in Hatton, James, and Swire[66] as proposed by Van Der Hegge Zjijnen, and the function put forward by Bruun[68]. This function is a polynomial in the square root of velocity.

$$E^2 = A + B \times (V^{0.5}) + C \times (V^{0.5})^2 + D \times (V^{0.5})^3 + \ldots \qquad (35)$$

This is an empirical function, which has not been attempted past second order.

Due to the peculiarities of the experiment, and the accuracy needed for boundary layer measurements, most calibrations in this study were performed in the wind tunnel. Since the properties of hot wires change with time due to age and dust deposition, which can be accelerated by particles left in the wind tunnel after particle drag tests, all flow measurements with a hot-wire were immediately preceded by a calibration against a pitot-static probe. This also obviated the need to make temperature corrections to the probe calibration, and prevented perturbation of the electronics which are themselves sensitive to ambient temperature, line voltage, and the impedance of the connections to the hot-wire probe. As the fan speed of the wind tunnel was variable from engine speed down to an extremely slow rotation, it was possible to get many calibration point over the velocity range of interest. Due to limitations on the sensitivity of the manometer used with the pitot-static probe, the lower limit of velocity readings was about 15-20 feet per second. Knowing the voltage reading of the hot-wire anemometer at each velocity, a

least squares fit of the desired calibration function can be performed[57]. Since a large amount of data was taken in the wind tunnel, statistical analysis can be performed with some confidence of meaningful results. Additionally, some data taken on a DISA Model 1125 Calibrator provides a check that the wind tunnel results are valid.

The best measure of the suitability of a functional fit is a standard deviation derived from known data and the calibration function, calculated using least squares procedures[69]. Given enough sets of calibrations and the derived standard deviations, it is possible to determine a 95% level of confidence for the standard deviation. Put another way, there is a fair level of certainty that 95% of all standard deviations of similar calibrations will be less than the 95% confidence level. Given this analysis, different calibration methods can be evaluated with respect to their statistically expected deviation, and with respect to each other. Of secondary consideration, but wider application, is the statistical expected error itself, defined as 67.45% of the standard deviation of the errors by assuming a so-called normal distribution of the error. The expected error does not take into account the variability of the error of calibration, as the confidence level does. A plot of a typical calibration is shown in Figure 21, with a fitted King's Law calibration function.

A PL/I[70] program was written to perform calibration regressions and data reduction using the three families of calibration functions. This is used to perform arbitrary power-law fits of calibration data, up to fourth order polynomial function fits, or up to third order King Series function fits. The self-documenting and machine-independent features of the language prompted its use. A copy of the source code of the program is included in Appendix C.

In order to eliminate blatantly bad calibrations from consideration, a criteria is defined that each set of calibration data must meet. For data from the wind tunnel, if no single function fit can produce better than 0.9 feet per second standard deviation

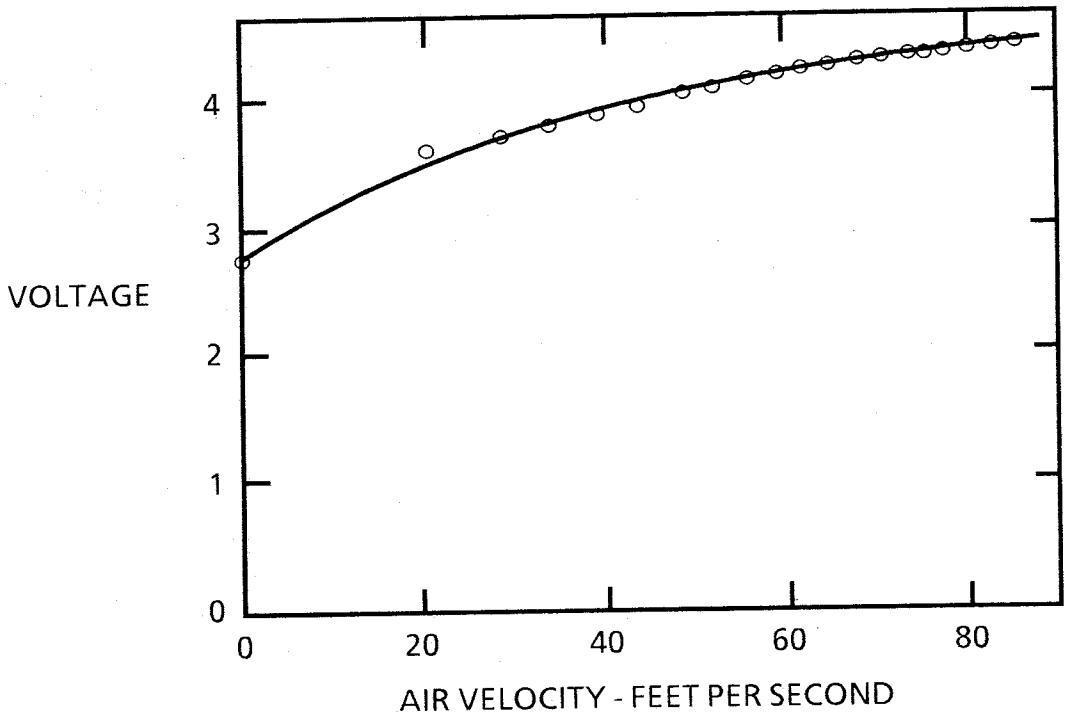


Figure 21 - Typical Set of Hot-Wire Calibration Data Points

calibration fit. then that set of calibration data is omitted from the analysis. Since the accuracy of the calibrator device is much better, the criteria is more stringent, as the data set must produce a calibration fit with better than 0.5 feet per second deviation. In this manner the statistical analysis is not biased towards a particular calibration function.

In the basic analysis of calibration accuracy, 32 data sets are available, of which 26 pass the criteria. This data is available in the Mechanical and Aerospace Engineering Department Library at the University of Missouri-Rolla[71]. It should be noted that two probe types were used in the test. Thirteen tests were conducted with DISA 55.A.22 probes and nineteen tests were conducted with DISA 55.F.14 probes. The standard deviations and confidence levels of the wind tunnel calibrations are shown in Figure 22. According to this data reduction, the fourth-order polynomial function is by far the most accurate. The fourth order polynomial has 30% of the confidence level of King's Law, about 40% of the confidence level of the best power-law fit, and about 70% of the

confidence level of the next best calibration function. Since the confidence level is based on the Student T distribution, it is more appropriate for small sample sizes and the confidence level will henceforth be referred to as the error. The fourth order polynomial has an error of 0.46 feet per second and an expected error of 0.27 feet per second. Figure 22 illustrates the basic accuracy of all wind tunnel data used in this investigation.

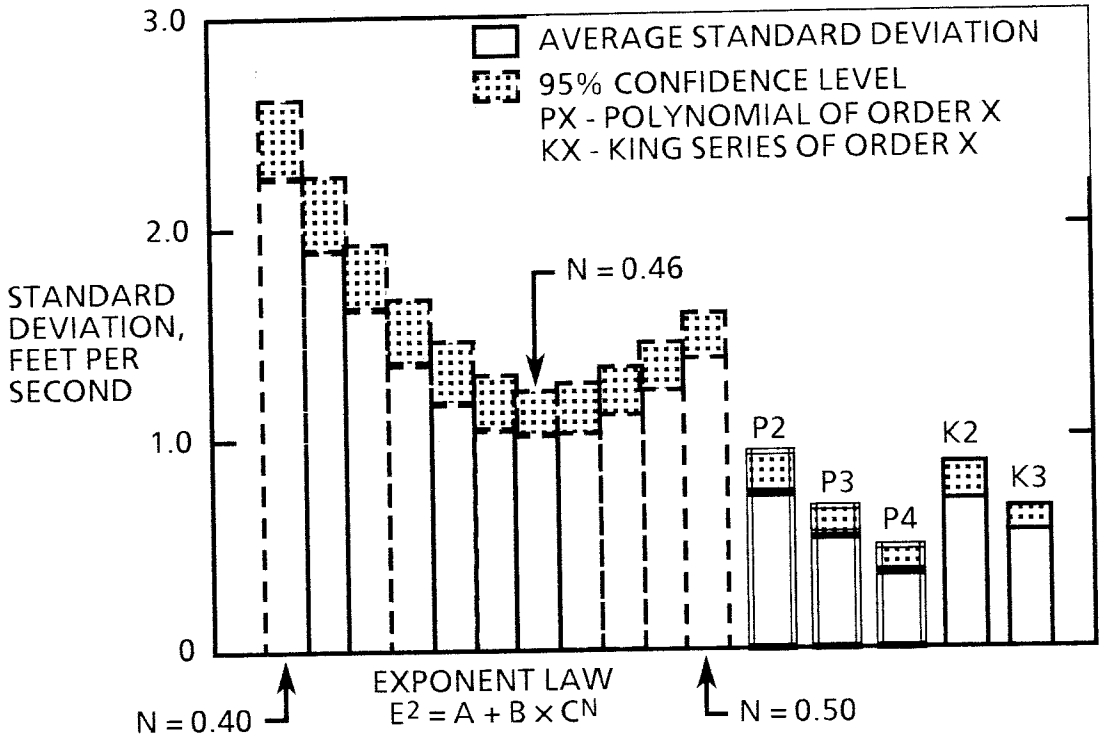


Figure 22 - Standard deviation and confidence level for all wind tunnel hot-wire calibrations, for various calibration functions

Before a clear picture of the suitability of the different calibration functions can be drawn, it is necessary to consider more than the simple raw error of calibration. In this case, at zero velocity the voltage reading squared is identical to the zero velocity constant 'A', which forms an outlaying data point. The results shown by Hatton, James, and Swire[66] indicate that static errors due to free rather than forced convection are below consideration for velocity calibrations of this magnitude, so this should be a condition amenable to accurate measurement. Furthermore, it forms an extreme condition at the

low end of the velocity scale, such that errors in the fit of the zero velocity constant 'A' to actual readings should be indication of actual error in low velocity portions of the calibration function fit. Figure 23 presents the standard deviation of 'A' to the known

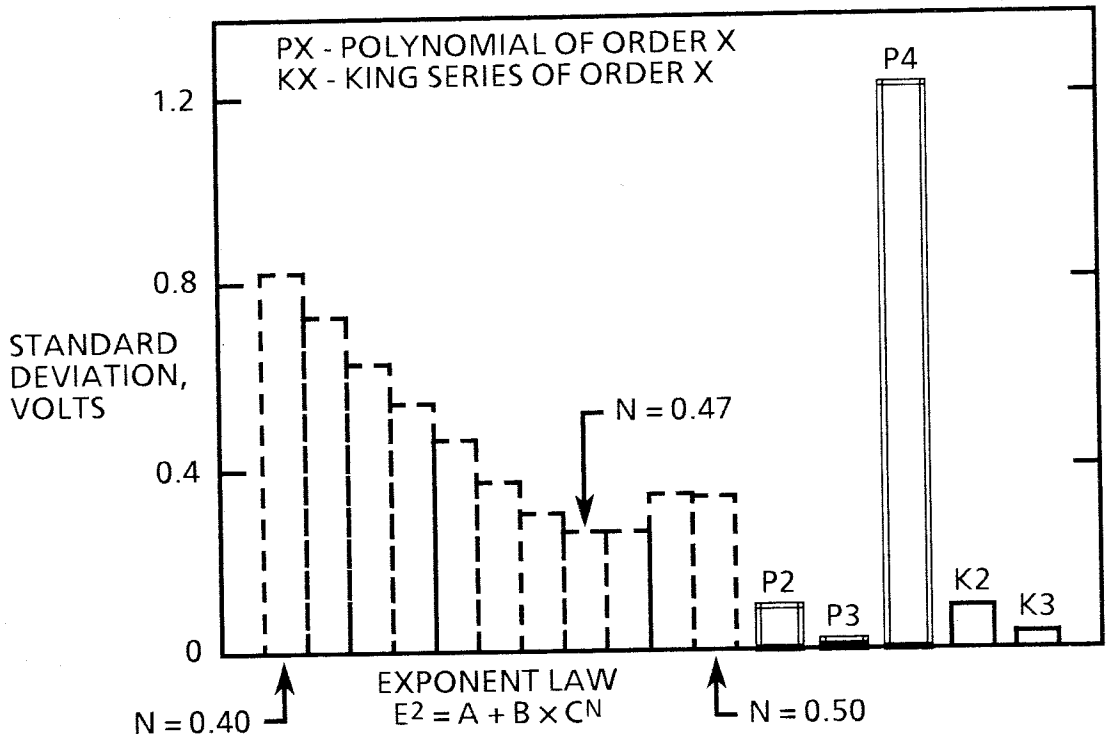


Figure 23 - Calibration function fit of zero velocity constant 'A', a reliable outlaying data point

value of voltage reading squared for the accepted wind tunnel calibrations. The trends are approximately the same as for the entire error of calibration, except for the third and fourth order polynomial functions. Apparently, the fourth order function is unstable, like many high-order functions, and does not fit the extreme point of the zero velocity datum. The analysis shows the third order polynomial to be the most stable and the most accurate near the low velocities. It can also be seen that the preferred power-law exponent is now 0.47 . On the basis of this test, the preferred calibration function for the wind tunnel data is the third order polynomial, especially in boundary layer measurements.

It is useful to know if the results of the wind tunnel calibration can be duplicated on a static calibration device which has more closely controlled conditions. Out of the four calibrations performed, three passed the more stringent acceptance criteria. It must be emphasized that such a small sampling does not provide a good basis for exact determination of the best calibraton function, but only an indication of the trends and a comparison of error of the wind tunnel calibration with more accurate calibration data sources. The results of this reduction are shown in Figure 24. The same general trends

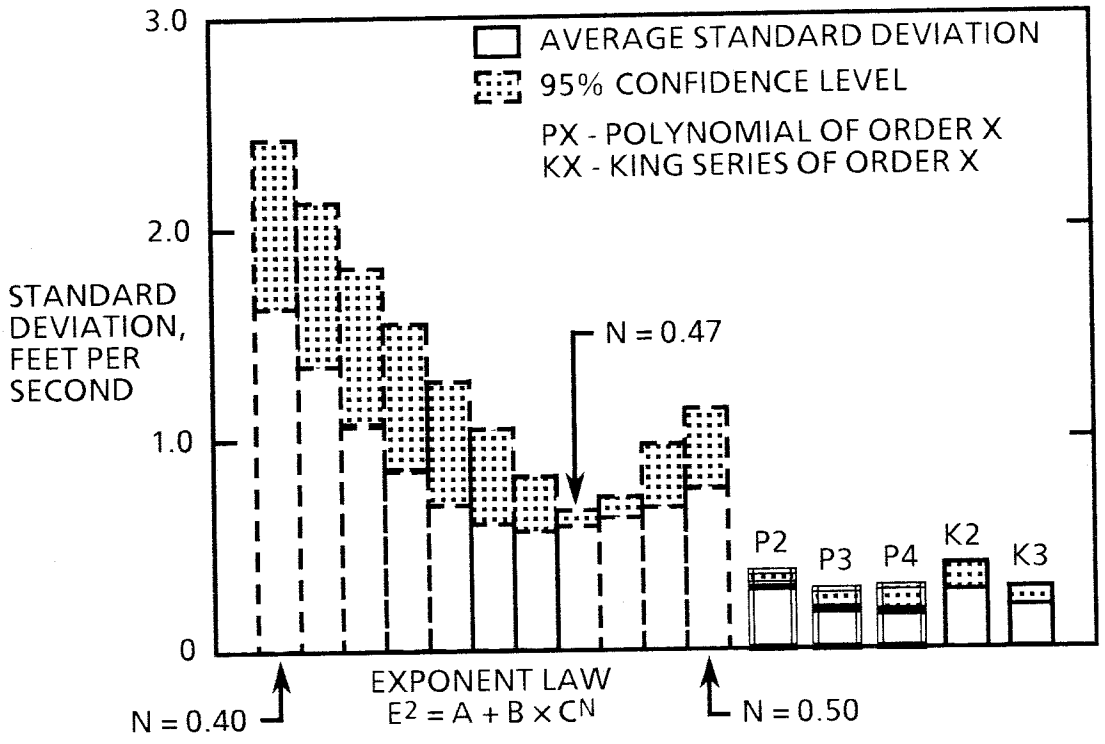


Figure 24 - Standard deviation and confidence for hot-wire calibration with DISA precision calibrator

apply with the calibrator as with the wind tunnel, with an error reduction of as much as two-thirds compared to the wind tunnel. Oddly enough, the third order polynomial is shown to be superior to the fourth order polynomial. Figure 25 illustrates the analysis of the zero velocity constant, and the fourth order polynomial is shown to be superior for

low velocities. It is possible that a larger sample size could modify the differences shown in this analysis between third and fourth order polynomial functions.

On the basis of the preceding tests, the polynomial function of order three was chosen to interpret the data taken by hot-wire anemometer during the course of the investigation. This function provides an expected error of 0.37 feet per second with much less sensitivity to noise than the fourth order polynomial. It has the best low velocity fit and its choice is consistent with the trends indicated by the static calibrator tests.

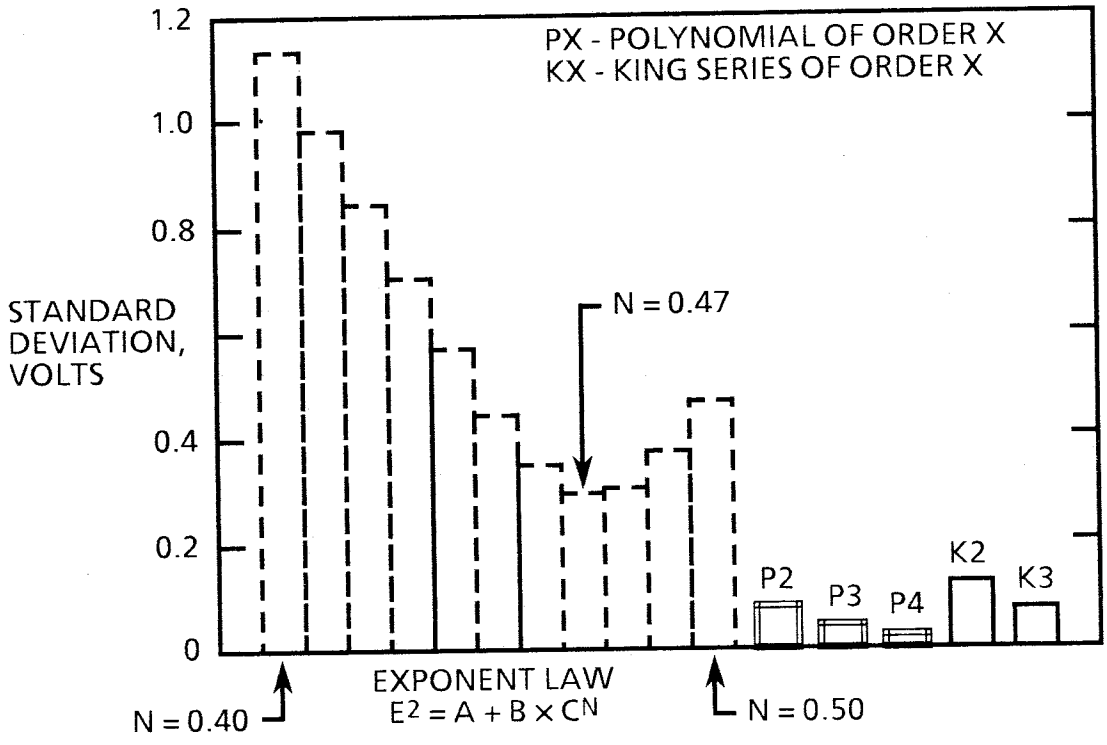


Figure 25 - Fit of zero velocity constant 'A' with calibrations performed on DISA precision hot-wire calibrator

C. LEADING EDGE SEPARATION

It is undesirable in this study to subject the test plate boundary layer flow to leading edge separation. This phenomena can distort the boundary layer in unpredictable ways. Drag measurements over portions of flat plates experiencing leading edge separation are meaningless. As the plate system involved in the present investigation is intended for turbulent boundary layer drag measurements, prevention of separation is absolutely vital. In order to determine the effects of particles on the turbulent boundary layer, distortion arising from separation could not be allowed.

Early in the history of boundary layer experiments Dryden[16] noted that care had to be taken with the flow at the leading edge of flat plates for boundary layer experiments. Dryden also found that the plate leading edge geometry played an extremely significant role. His results indicated that a symmetrical leading edge had to be used for sharp, thin test plates, and even with that geometry alignment of the plate with the flow was very critical. This result was also obtained in the present study, shown in Appendix B.

Davis[30] showed optimum parameters for two blunt or rounded leading edge forms that could be used to provide stable development of boundary layers on flat plates. A leading edge fairing was designed for this study's test plate which followed Davis' recommendations (Figure 26). As development of the leading edge and pressure gradient

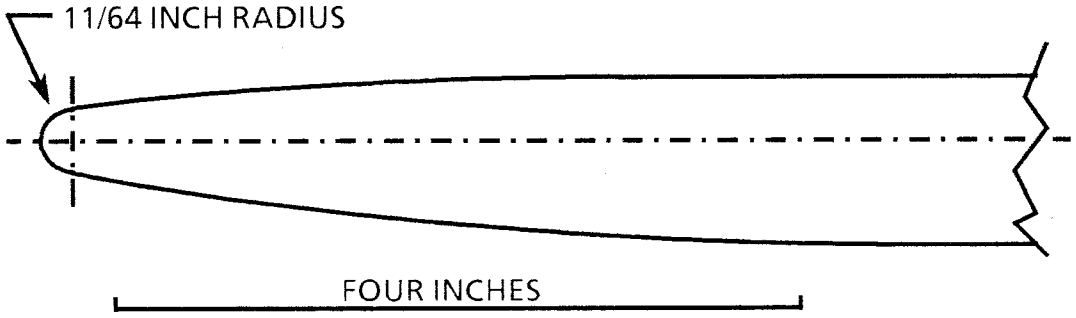


Figure 26 - Plate system leading edge fairing contour.

treatment progressed, it became apparent that, if the boundary layer thickness approached that of a laminar boundary layer, then separation would be minimal or nonexistent. A comparison of the boundary layer profile with boundary layer thickness computed from the Blasius equations indicates that separation has been avoided, even on an unsymmetrical leading edge design (Figure 27).

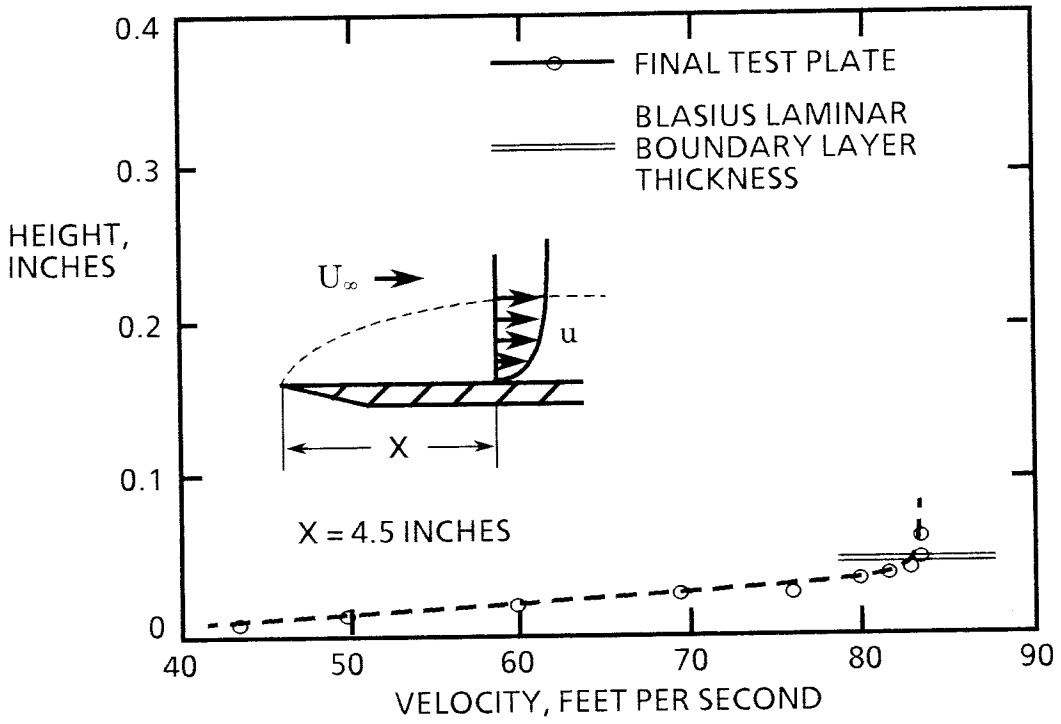


Figure 27 - Comparison with laminar boundary layer thickness.

D. NOZZLE AND NOZZLE SUPPORT INTERFERENCE

One requirement peculiar to this test of a boundary layer with particle injection is an injection nozzle upstream of the test plate. Naturally, the nozzle should not interfere with the natural development of the boundary layer, but it is in the best position to do so. A primary concern in the development of the experiment was a stable dispersal of particles from the nozzle in an accurate trajectory over the test plate surface. In order to do this the nozzle was mounted in the settling chamber of the wind tunnel, extending into the diffuser and terminating three feet, ten and one-half inches from the leading edge of the plate system. The nozzle was supported near its end by streamlined support strut from the lower wall of the test section diffuser as noted in Apparatus and Appendix B. Earlier nozzle support designs had produced wakes that interfered with the flow field on the top test plate, either by producing a wake velocity deficit imposed on the boundary layer profile, or by increased turbulence level. This data is shown in Appendix B. In order to eliminate even the turbulent wake effects while the nozzle was inoperative, the nozzle geometry was designed with an upward slant to project the particle stream to the test plate. During tests without particle injection, the wake of the nozzle and support strut passes underneath the test plate, reducing interference in this case. Exploration of the flow over the top of the test plate with a hot-wire anemometer confirmed that the turbulent wake of the nozzle was not interfering with the uppper boundary layer. However, it must be noted that the presence of the particle injection machinery, the plate system, and the hot-wire traverse has increased the general turbulence level of the free stream (Figure 28).

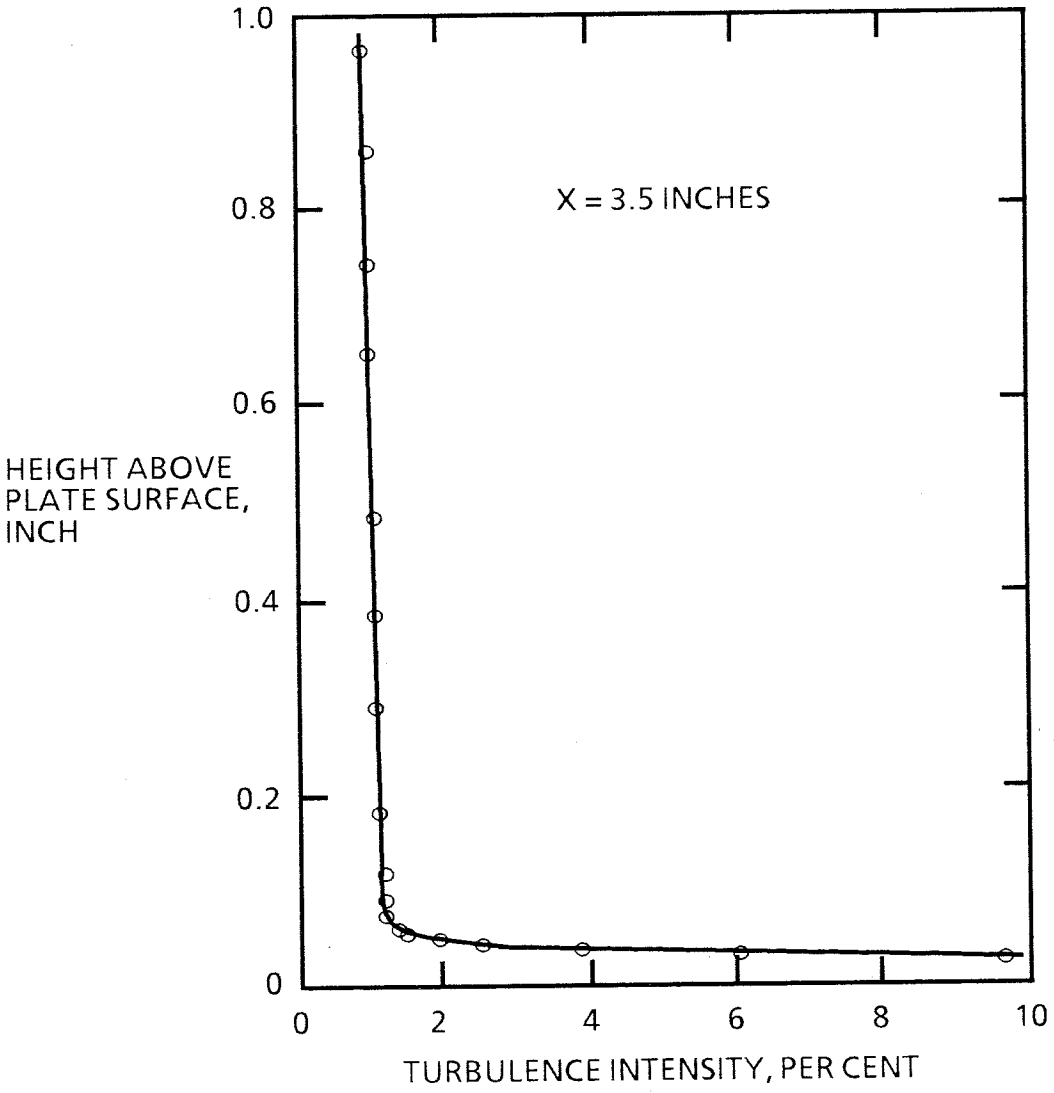


Figure 28 - Turbulence above test plate with final nozzle geometry.

## E. BOUNDARY LAYER FLOW OVER THE TEST PLATE

It is important to review the basic questions of the experiment relative to boundary layer flow over the plate, and the factors influencing that flow. It was to be determined if the boundary layer of the test plate was of an equilibrium nature, existing in a reasonably uniform static pressure field, and conforming to a non-distorted turbulent boundary layer as defined by previous investigators. This concern did not extend to the entire plate system, but only to the test plate surface and the leading edge fairing upstream of it. Factors which have been shown to affect these qualities are the pressure gradient over the plate system, turbulent wakes impinging on the plate leading edge, leading edge shape, free-stream turbulence, plate surface roughness, and the edges of the plate. The data gathered for this analysis is available at the Department of Mechanical and Aerospace Engineering Library of the University of Missouri-Rolla[72].

Normally the plate surface is treated with sandpaper roughness on the leading edge for the purpose of increasing boundary layer thickness for the optical instruments involved in particle drag reduction tests. This roughness was removed to achieve a smooth surface and determine the quality of the leading edge flow and the point of transition of the boundary layer without surface treatment. Figure 29 through Figure 33 are plots of the boundary layer velocity profiles at the plate centerline compared to the Blasius solution of the boundary layer profile for a laminar boundary layer. Although the traverse apparatus was not originally designed for the demanding accuracy required for thin laminar boundary layers excellent agreement is shown to a Reynolds Number of about 20000. It was determined that wall corrections were not necessary for this apparatus by moving the probe close to the test plate at zero air velocity. The boundary layer is free from intermittent separation and undergoes transition to a turbulent boundary layer at about seven inches from the leading edge of the plate, or close to the gap between the leading edge fairing and the test plate. This gap apparently triggers the

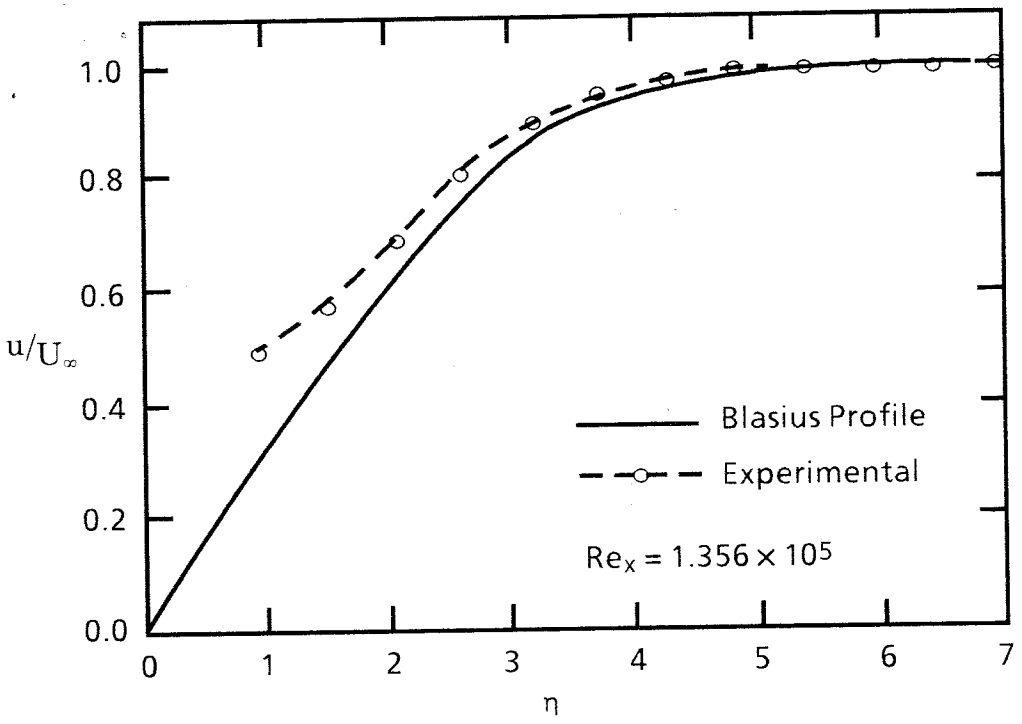


Figure 29 - Boundary layer profile at x = 3.5 inch

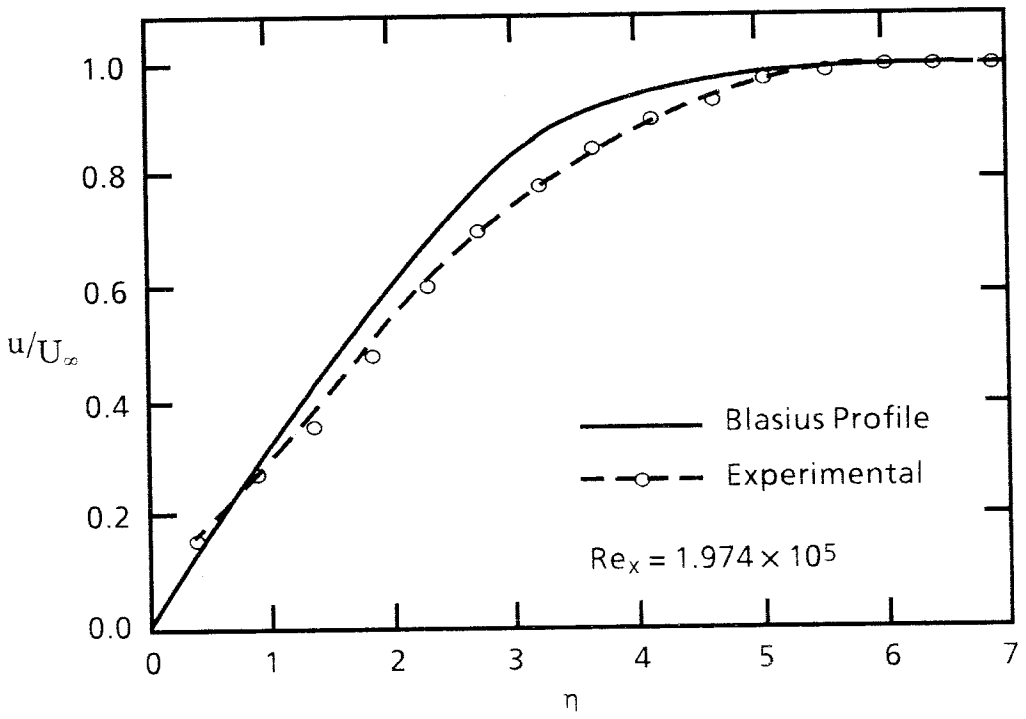


Figure 30 - Boundary layer profile at x = 5.0 inch

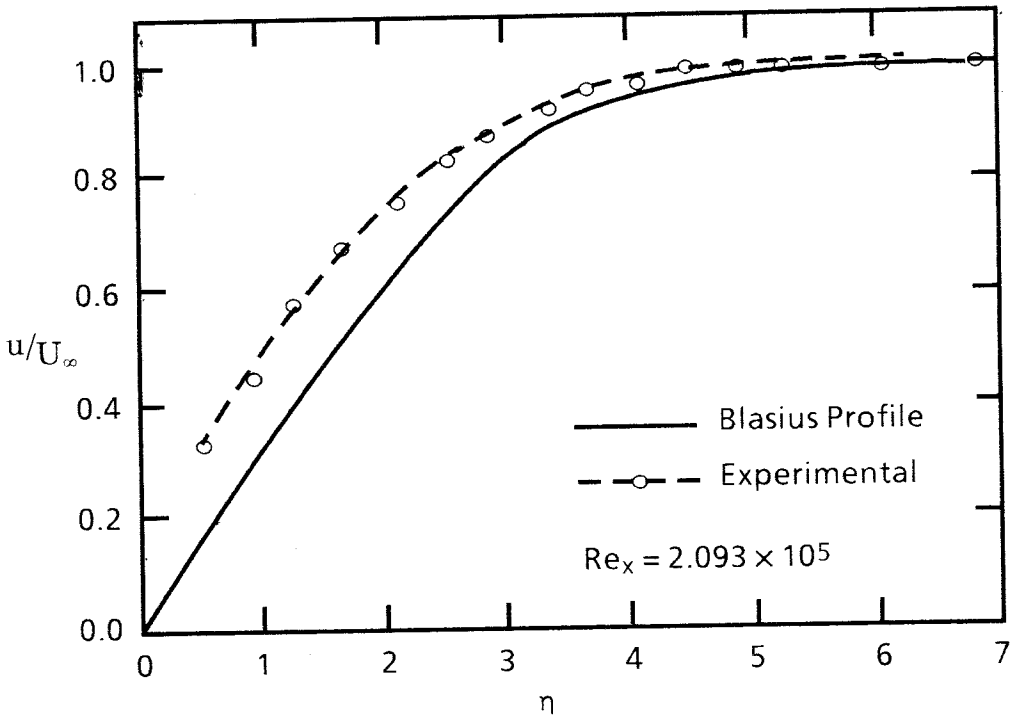


Figure 31 - Boundary layer profile at x = 6.0 inch

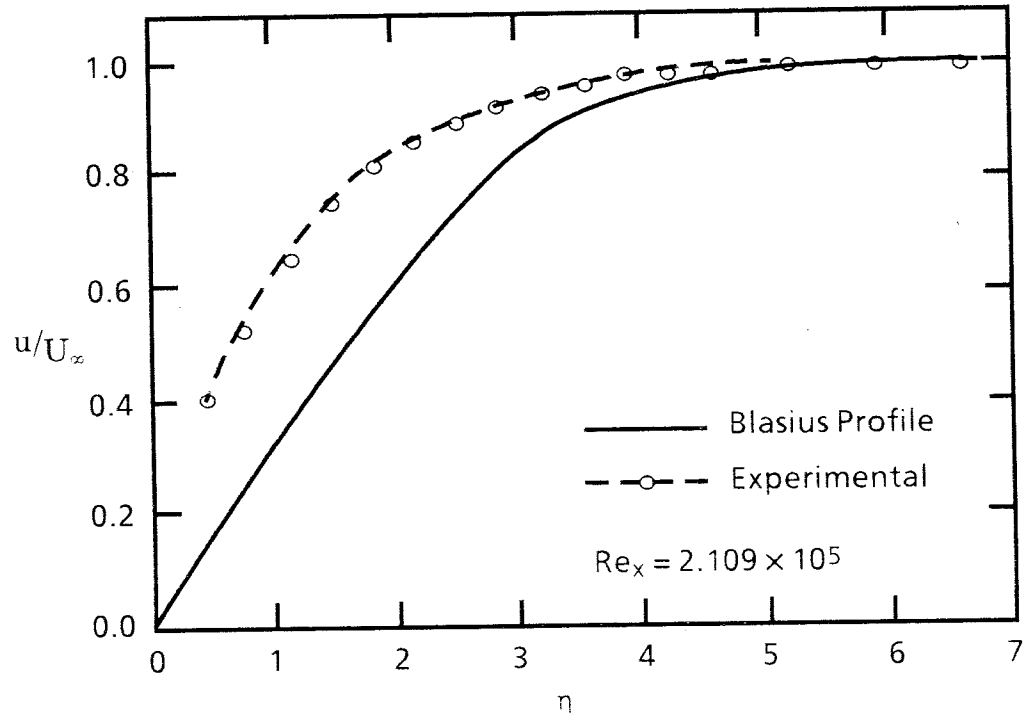


Figure 32 - Boundary layer profile at x = 7.0 inch

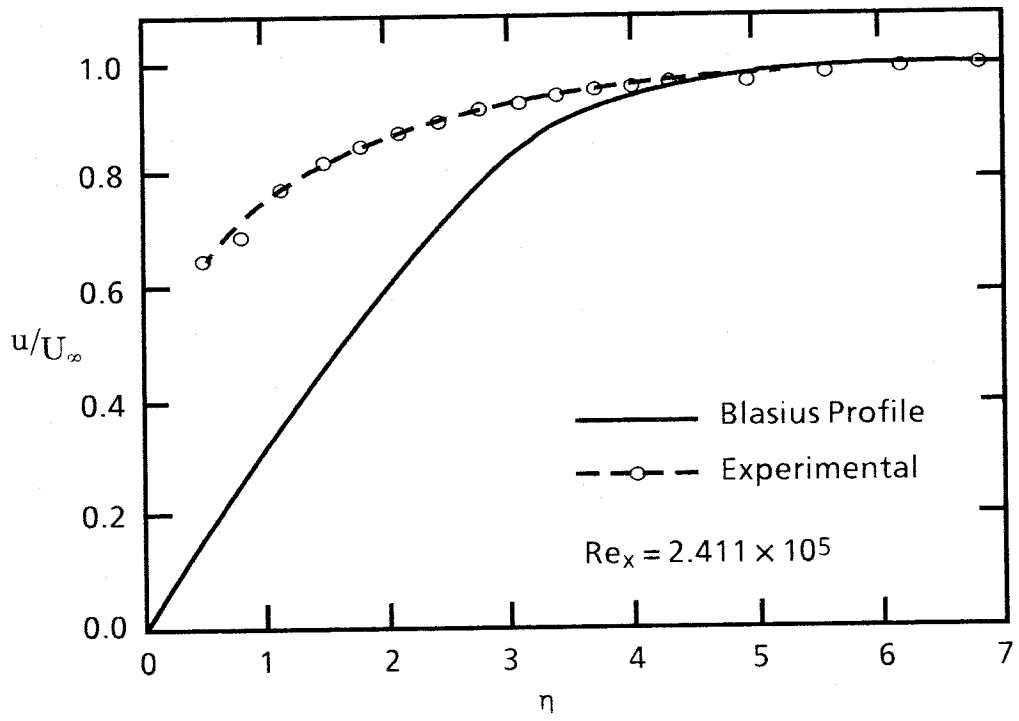


Figure 33 - Boundary layer profile at x = 8.125 inch

transition before the normal Reynolds Number range of 35000 to 50000 determined by other investigators.

Preliminary testing of boundary layer properties across the test plate revealed uniform properties with respect to profile shape, momentum and displacement thickness, and friction coefficient as derived from the law of the wall relation. Tests by Elder[32] have shown that three dimensional disturbances originating at the edges of a finite width plate tend to spread inward at about eight to ten degrees from the sides (these experiments were conducted on rectangular plates of low aspect ratio with the long edges aligned with the flow). In the test plate some crossflow and distortion of the two dimensional properties of the boundary layer might be expected over the test plate area about 50 inches from the leading edge of the plate. Figure 34, however, show that no great difference between the boundary layer at the centerline of the plate and 4.28 inches from the centerline was present.

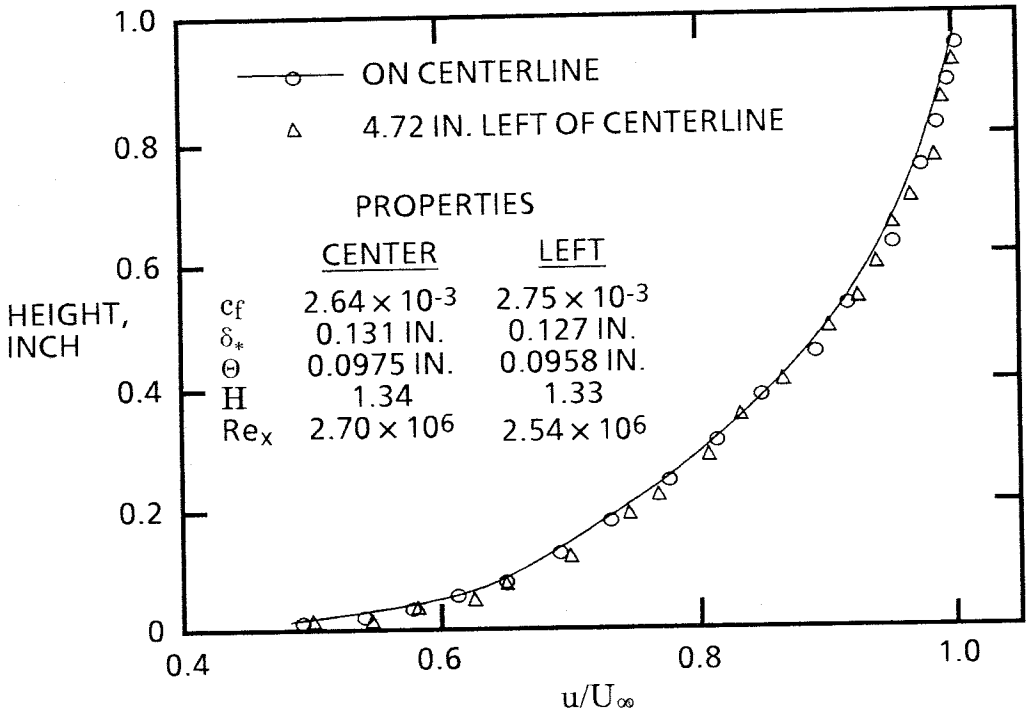


Figure 34 - Variation of velocity profile across plate at x = 59.75 inches, smooth leading edge

With the sandpaper roughness applied near the leading edge of the plate system, both the nature of the turbulent boundary layer along the centerline and across the plate was investigated. Of primary concern is the effect of the sandpaper roughness on the turbulent boundary layer. The investigations of Klebanoff and Diehl showed that such roughness could drastically distort the boundary layer flow, preventing formation of an equilbrium turbulent boundary layer to quite high Reynolds Numbers. Figure 35 shows that the particular roughness applied to the plate system (6 inches of Number 40 sandpaper applied with its leading edge one inch downstream of the plate system leading edge) did distort the turbulent boundary layer. The boundary layer is effectively in equilibrium at a Reynolds Number of about 600000, a small Reynolds Number and equivalent to a short distance on the test plate at the nominal wind tunnel velocities. The major effect of the sandpaper roughness was in increasing the thickness of the boundary layer, equivalent to adding a 14 inch leading edge extension to the plate system.

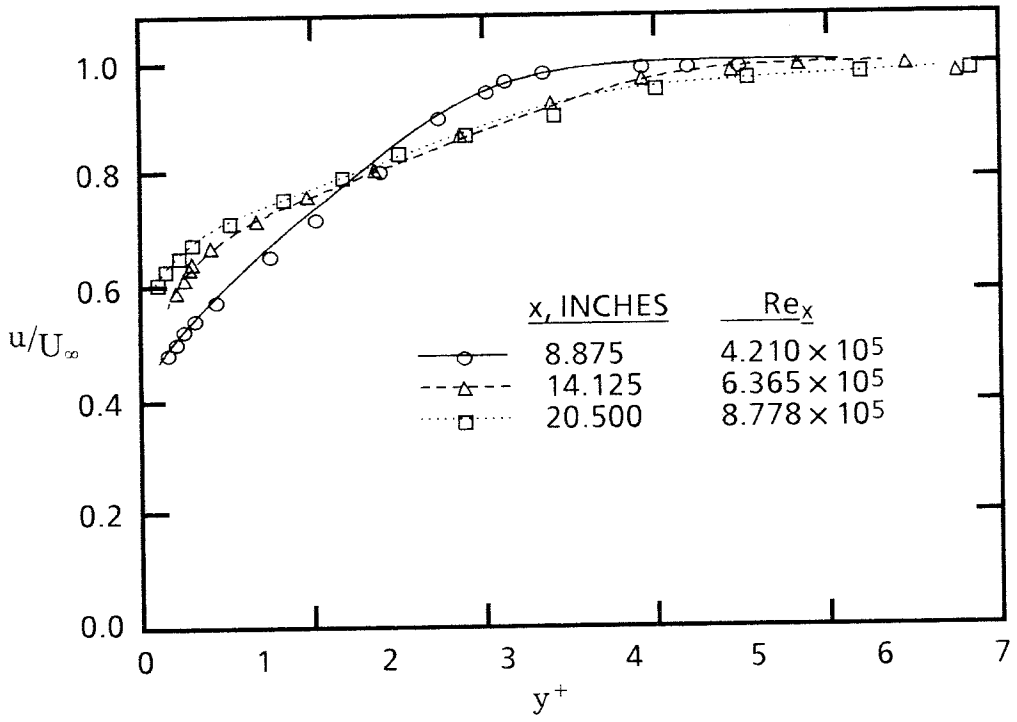


Figure 35(a) - Boundary layer profiles with roughness applied to plate.

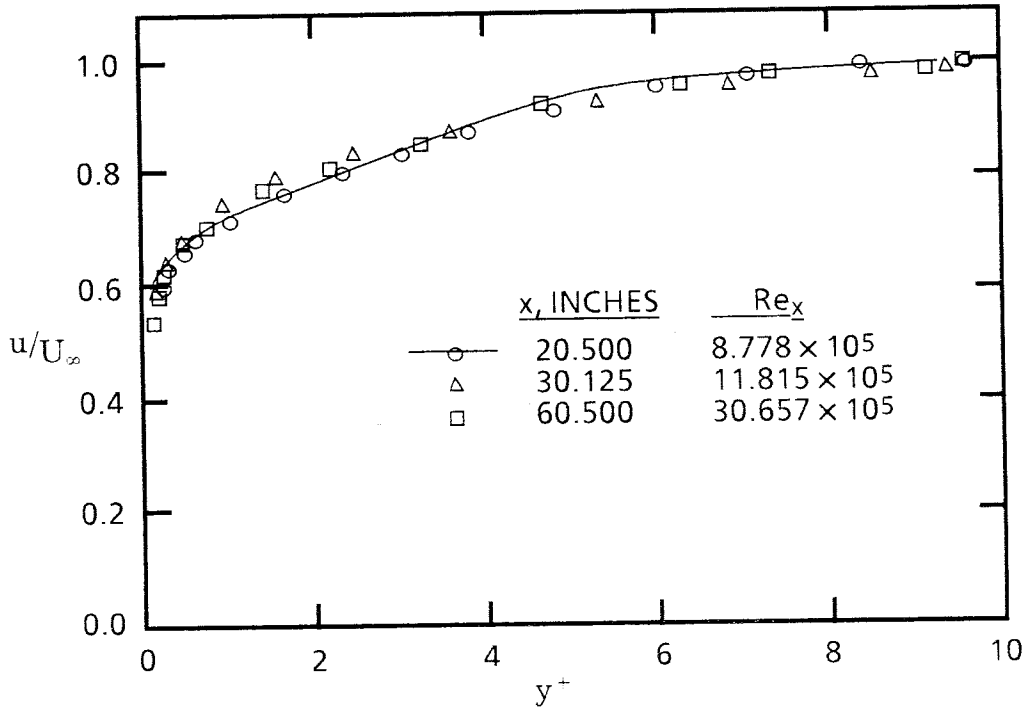


Figure 35(b) - Boundary layer profiles with roughness applied to plate.

The investigations of Elder were not concerned with the effect of roughness on the edge influence on the boundary layer over a finite flat plate. Therefore, a traverse across the plate was performed with the leading edge roughness in place to determine if the roughness would destroy the two-dimensional nature of the flow over the test plate. Figure 36 shows that the boundary layer properties across the plate are in good agreement, as in the case without the leading edge roughness.

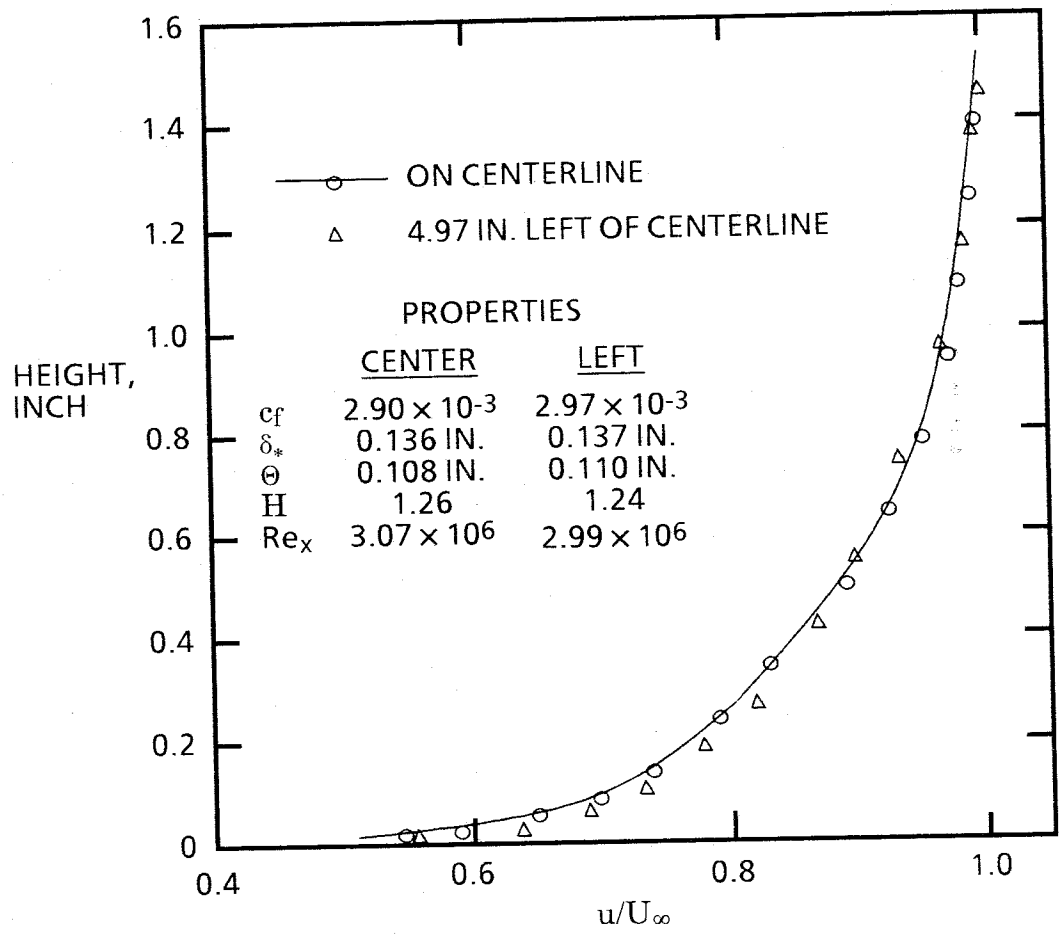


Figure 36 - Variation of velocity profile across plate at x = 60.50 inches, roughness applied to plate leading edge.

Finally, as a confirmation that the boundary layer over the test plate conformed to results of other investigators as reported by Schlichting[17], a comparison is made of the present results to the so-called universal law of the wall. In this comparison, the

coefficients for the flat-plate turbulent boundary layer are used, namely A of 5.85 and D of 5.56 (see equation 22). Figure 37 shows excellent agreement with the universal law of the wall. There is, as noted by Schlichting, Clauser[20], and others, a velocity defect arising at about a $y^+$ of 1000. This is a deviation from the law of the wall in the outer region of the boundary layer, where the turbulent boundary layer is said to obey the law of the wake. Also, the laminar sub-layer, which does not follow the law of the wall, is not legible in the scale used.

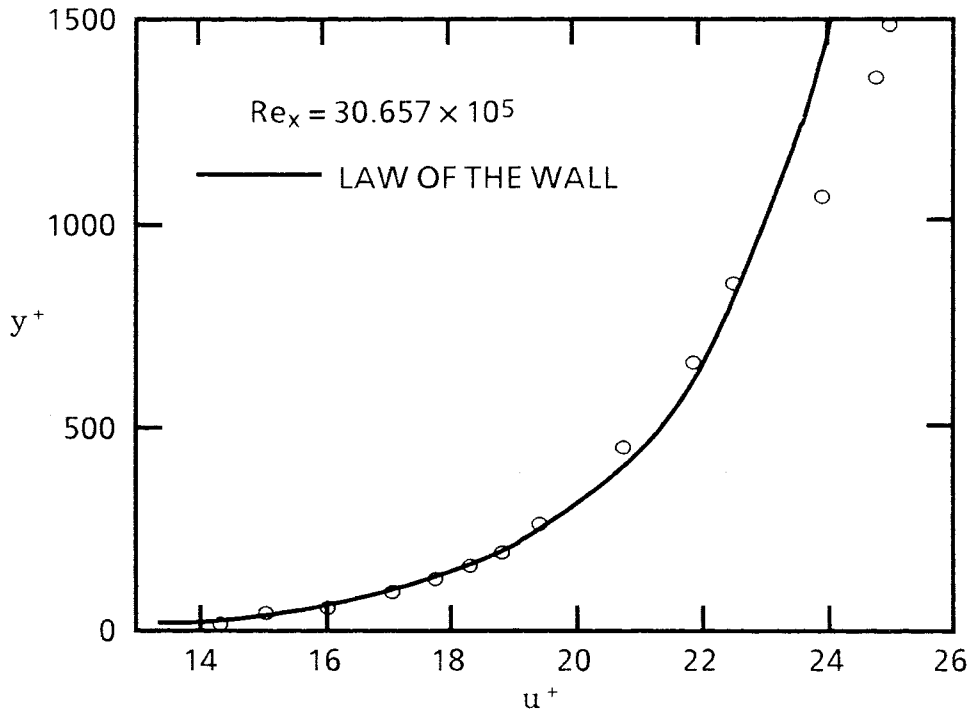


Figure 37 - Boundary layer profile at x = 60.5 inches compared to the Universal Law of the Wall